SCIENCE CHINA
Chemistry

•ARTICLES•

December 2020 Vol.63 No.12: 1777–1784
https://doi.org/10.1007/s11426-020-9819-4

A synchronous nucleation and passivation strategy for controllable synthesis of $Au_{36}(PA)_{24}$: unveiling the formation process and the role of $Au_{22}(PA)_{18}$ intermediate

Xiaoshuang Ma[1], Guanyu Ma[1], Lubing Qin[1], Guangxu Chen[1], Shaowei Chen[3*] & Zhenghua Tang[1,2*]

[1]*Guangzhou Key Laboratory for Surface Chemistry of Energy Materials and New Energy Research Institute, School of Environment and Energy, South China University of Technology, Guangzhou 510006, China;*
[2]*Guangdong Engineering and Technology Research Center for Surface Chemistry of Energy Materials, School of Environment and Energy, South China University of Technology, Guangzhou Higher Education Mega Centre, Guangzhou 510006, China;*
[3]*Department of Chemistry and Biochemistry, University of California, 1156 High Street, Santa Cruz, California, 95064, United States*

Received June 23, 2020; accepted July 7, 2020; published online September 1, 2020

Despite the recent progress on controllable synthesis of alkynyl-protected Au nanoclusters, the effective synthetic means are very limited and the cluster formation process still remains puzzling. Here, we develop a novel synchronous nucleation and passivation strategy to fabricate $Au_{36}(PA)_{24}$ (PA=phenylacetylenyl) nanoclusters with high yield. In $Au_{36}(PA)_{24}$ formation process, $Au_{22}(PA)_{18}$ as key intermediate was identified. Meanwhile, $Au_{22}(PA)_{18}$ can be synthesized under a low amount of reductant, and by employing more reductants, $Au_{22}(PA)_{18}$ can turn into $Au_{36}(PA)_{24}$ eventually. Moreover, the structure evolution from $Au_{22}(PA)_{18}$ to $Au_{36}(PA)_{24}$ is proposed, where four Au_{13} cuboctahedra can yield one Au_{28} kernel. Finally, the ratiocination is verified by the good accordance between the predicted intermediate/product ratio and the experimental value. This study not only offers a novel synthetic strategy, but also sheds light on understanding the structural evolution process of alkynyl-protected Au nanoclusters at atomic level.

synchronous nucleation and passivation, $Au_{36}(PA)_{24}$, $Au_{22}(PA)_{18}$, unveiling the formation process, structure evolution, intermediate/product ratio

Citation: Ma X, Ma G, Qin L, Chen G, Chen S, Tang Z. A synchronous nucleation and passivation strategy for controllable synthesis of $Au_{36}(PA)_{24}$: unveiling the formation process and the role of $Au_{22}(PA)_{18}$ intermediate. *Sci China Chem*, 2020, 63: 1777–1784, https://doi.org/10.1007/s11426-020-9819-4

1 Introduction

Atomically precise coinage metal nanoclusters with molecular purity have been gaining tremendous research attention in the past decade [1–8], as their well-defined structures provide an ideal platform to establish the relationship between the structure and the physiochemical properties including luminescence [5,9,10], catalytic reactivities [6,11,12], electrochemical behaviors [13], and biomedical capabilities as biolabeling agents [14] or biomarkers [15,16]. The last decade has witnessed the great success on controllable synthesis and structural determination of thiolate Au nanoclusters, as more than 200 cluster structures have been revealed by single crystal X-ray diffraction (SCXRD). However, for homoleptic alkynyl-protected Au nanocluster counterparts, despite the recent progress of several examples including $Au_{22}L_{18}$ (L–H=3-ethynylthiophene, phenylacetylene, 3-ethynyltoluene, 3-ethynylanisole, and 3,3-dimethyl-1-butyne) [17,18], $Au_{23}L_{15}$ (L–H=3,3-dimethyl-1-butyne) [19], $Au_{25}L_{18}$ (L=3,5-bis(trifluoromethyl)phenyl) [20],

*Corresponding authors (email: shaowei@ucsc.edu; zhht@scut.edu.cn)

$Au_{36}L_{24}$, $Au_{44}L_{28}$ (L–H=phenylacetylene) [21], $Au_{42}L_{22}$ (L–H=2-(trifluoromethyl)phenylacetylene) [22], $Au_{50}L_{26}$ (L–H=3-fluorophenylacetylene) [22], $Au_{144}L_{60}$ [23], (L–H=1-ethynyl-2-fluorobenzene), the family numbers with defined structure are still rare, presenting great promises in this burgeoning field. Several factors can account for this. First of all, the current synthetic approaches are very limited (mainly direct reduction of precursor by $NaBH_4$) [24–28], not to mention the low yield. For instance, through the direct reduction approach, the yield of $Au_{36}(PA)_{24}$ (PA=phenylacetylenyl) was only ~5% [21], while the yields of $Au_{22}(PA)_{18}$ [17] and $Au_{22}(^tBuC{\equiv}C)_{18}$ [18] were ~8% and ~29%, respectively. Secondly and more importantly, the formation process of molecular alkynyl Au nanoclusters is still puzzling, as most of the research attention has been paid to total structure elucidation of the nanoclusters.

Note that, although alkynyl Au nanoclusters somewhat resemble thiolate Au nanocluster counterparts [29], yet alkynyl molecule has different bonding modes on Au surface from thiolate ligand (*i.e.*, π-binding motifs) [30–34]. Plus its more reactive self-oligomerization behaviors (*e.g.*, alkynyl can form dimer and tetramer, while thiols only form disulfides) [35], these factors have imparted the precursor being extremely difficult to be identified and manipulated, resulting in the product being more diverse and complicated. To discover more members in alkynyl Au nanoclusters, developing more effective synthetic approaches and unveiling the cluster formation process is imperative. The following questions can be immediately asked: (1) Can we develop some new methods for controllable synthesis of alkynyl-protected Au nanoclusters with high yield? (2) What is the nanocluster formation process at atomic level? Can we isolate some reaction intermediates? By identifying the key intermediate, can we eventually unveil the structural evolution process of the final product? These questions form our aim and goal of our current investigation.

Here, we develop a novel synchronous nucleation and passivation strategy to fabricate $Au_{36}(PA)_{24}$ nanoclusters with high yield (>17%) by using $NaBH_3CN$ as reducing agent at low temperature. In the formation process of $Au_{36}(PA)_{24}$ (Au_{36} in short), $Au_{22}(PA)_{18}$ (Au_{22} in short) as key intermediate was identified. The structure of Au_{36} was confirmed by SCXRD, while the composition of Au_{22} was revealed by matrix-assisted laser desorption ionization mass spectrometry (MALDI MS). Note that, Au_{22} can also be isolated as the product when a low amount of $NaBH_3CN$ was employed, and by increasing the stoichiometry of $NaBH_3CN$/Au, Au_{22} can turn into Au_{36} eventually while too much reductant only yielded polydisperse Au nanoclusters. Finally, the structure evolution from Au_{22} to Au_{36} has been proposed, where Au_7 kernel plus $Au_6(PA)_6$ ring can form Au_{13} cuboctahedron and four Au_{13} cuboctahedra interpenetrate with each other, leading to the formation of one Au_{28} kernel in Au_{36} eventually. The above ratiocination was confirmed by the good accordance between the predicted intermediate/product ratio and the experimental value.

2 Experimental

2.1 Materials and reagents

Chloroform, ethanol, dichloromethane, and *n*-hexane were purchased from Caiyunfei Chemical Reagents (Tianjin, China). Phenylacetylene (HC≡CPh), 1,3-bis(diphenylphosphino)propane, 2-thiapropane (Me_2S), anhydrous triethylamine (Et_3N, 99.5%), and hydrogen tetrachloroaurate(III) trihydrate ($HAuCl_4{\cdot}3H_2O$) were acquired from Energy Chemicals (Shanghai, China). Sodium cyanoborohydride ($NaBH_3CN$) was obtained from Aladdin Industrial Corporation (Shanghai, China). The water with the resistivity of 18.3 MΩ cm^{-1} was supplied by using a Barnstead Nanopure water system. All chemicals were used as received without further purification.

2.2 Synthesis

2.2.1 *Synthesis of Me_2SAuCl*

Me_2SAuCl was synthesized according to the procedure described by Russell *et al*. [36]. Briefly, under Ar atomosphere, a solution of Me_2S (0.65 mL, 8.82 mmol) in anhydrous ethanol (30 mL) was added directly to $HAuCl_4{\cdot}3H_2O$ (1.00 g, 2.94 mmol) dissolved in anhydrous ethanol (20 mL) with vigorous stirring (1,000 r min^{-1}), where white precipitates began to form immediately. The mixture was kept stirring at room temperature for 2 h until the aqueous phase turned into colorless. The solution was cooled to 0 °C for 10 min, and the white precipitates were isolated by filtration, washed with cold ethanol (3×10 mL) and dry diethyl ether (3×10 mL). The product was a white solid without drying (yield, 95%).

2.2.2 *Synthesis of the $Au_{22}(C{\equiv}CPh)_{18}$ nanoclusters (Au_{22})*

In a 100 mL flask, 30 mg Me_2SAuCl was dissolved in 50 mL $CHCl_3$ at ice-bath temperature under Ar atmosphere. Then, phenylacetylene and triethylamine (1 equiv. per Au) were added in $CHCl_3$ (solution A) under stirring. 2.1 mg $NaBH_3CN$ was dissolved in 1 mL pre-cooled EtOH (solution B). Subsequently, solutions A and B were synchronously added dropwisely in the Au(I) solution under vigorously stirring (1,024 r min^{-1}). During the addition course, the reaction mixture changed from colorless solution to orange red suspension and then to bright red solution. After that, the bright red solution was evaporated to give a red solid, which was successively washed with 3×10 mL MeOH and 3×10 mL hexane, followed by extraction with CH_2Cl_2 and then dried by rotary evaporation.

2.2.3 Synthesis of the $Au_{36}(C{\equiv}CPh)_{24}$ nanoclusters (Au_{36}) In a 100 mL flask, 30 mg Me_2SAuCl was dissolved in 50 mL $CHCl_3$ at an ice-bath under Ar atmosphere. Then, phenylacetylene and triethylamine (1 equiv. per Au) were co-dissolved in $CHCl_3$ (solution C). 6.3 mg $NaBH_3CN$ was dissolved in 1 mL pre-cooled EtOH (solution D). Subsequently, solutions C and D were synchronously added dropwise in the Au(I) solution under vigorously stirring (1,024 r min^{-1}). The reaction mixture was kept stirring at 0 °C overnight in the absence of light. Finally, the reaction solution turned into green. After that, the mixture was evaporated to give a dark solid, which was successively washed with 3×10 mL MeOH, 3×10 mL hexane and 3×5 mL ether. The crude products dissolved in 1 mL of CH_2Cl_2 were pipetted onto ten pieces of a preparative thin layer chromatography (PTLC) plate (10 cm by 20 cm), and the separation was conducted in a developing tank (solvent: CH_2Cl_2/*n*-hexane=1:2, *v*/*v*) for ~10 min. Then, the band of $Au_{36}(C{\equiv}CPh)_{24}$ (green) in the PTLC plate were cut, and the nanoclusters were extracted with pure CH_2Cl_2 and then dried by rotary evaporation. After diffusion of *n*-hexane to a dichloromethane solution at 4 °C for about 7 d, sheet-like single dark crystals were obtained.

2.3 Physical measurements and instrumentation

UV-visible (UV-Vis) absorption spectra were recorded on a Shimadzu 2600/2700 spectrophotometer (Japan). The metal-to-organic ratio of the Au nanoclusters was determined by thermogravimetry analysis (TGA) with a METTLER instrument (Switzerland) under N_2 atmosphere. Mass spectra were acquired with Ultrafle Xtreme matrix assisted laser desorption ionization time-of-flight (MALDI TOF-TOF) analyzer (Bruker, Germany) with *trans*-2-[3-(4-*tert*Butylphenyl)-2-methyl-2-propenylidene]-malononitrile (DCTB) as matrix. The surface chemical compositions and valence states were examined by X-ray photoelectron spectroscopy (XPS, Phi X-tool instrument, USA).

2.4 X-ray crystallography

Data collection for $Au_{36}(C{\equiv}CPh)_{24}$ was carried on an Agilent Technologies SuperNova Single Crystal Diffractometer using Mo Kα radiation (λ=0.71073) at 250 K. Absorption corrections were applied by using the program CrysAlis (multi-scan) [37]. The structure was solved by direct methods, and non-hydrogen atoms were refined anisotropically by least-squares on F^2 using the SHELXTL program. C atoms and solvent molecules were refined isotropically due to weak diffraction. The structure was solved and refined using full-matrix least-squares based on F^2 with program SHELXS-97 and SHELXL-97 within OLEX2 [38].

3 Results and discussion

3.1 Characterization of Au_{36} and identification of Au_{22} as key intermediate

In a previous study, Wang group [21] reported the crystal structure of $Au_{36}(PA)_{24}$, while the synthesis was conducted by the direct reduction of the Au:C≡CPh precursor using $NaBH_4$. Here, we develop a new synchronous nucleation and passivation method and the synthetic route for Au_{36} and the other products is illustrated in Scheme 1. Instead of adding the ligand first then the reducing agent, in our method, PA ligand and the reducing agent of $NaBH_3CN$ were simulta-

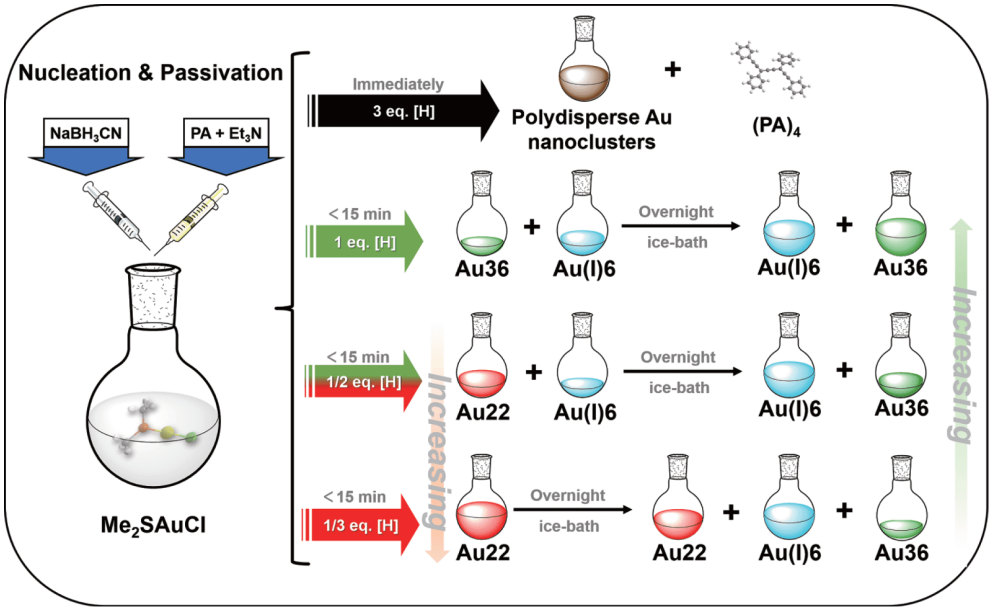

Scheme 1 The synthetic route of $Au_{36}(PA)_{24}$ nanoclusters by controlling different amounts of $NaBH_3CN$ (color online).

neously dropwise injected into the Me_2SAuCl solution in an ice-bath (See details in Experimental section). Black crystals were collected after diffusion of *n*-hexane to a dichloromethane solution and characterized by SCXRD. The composition of the final product was first revealed by MS. As shown in Figure 1(a), there is a sharp peak at 9,417.55 Da, corresponding well with $[Au_{36}(PhC{\equiv}C)_{23}]^+$ (theoretical molecular weight, MW: 9,416.74 Da, deviation: 0.81 Da). The summarized identification of the other major peaks in Figure 1(a) can be found in Table S1, where $[Au_{36}(PA)_{23}]^+$ and $Au_{32}(PA)_{20}^+$ are observable. In addition, the molecular structure elucidated by SCXRD is presented in Figure S1 (Supporting Information online) with the detailed structural parameters summarized in Table S2 (Supporting Information online). Moreover, $Au_{36}(PA)_{24}$ exhibits an absorption band at 640 nm and a broad hump at 405 nm (Figure 1(c)). The energy bandgap derived from the absorbance spectrum is ~1.65 eV (inset in Figure 1(c)). The combined MALDI-MS data and single crystal molecular structure, plus the characteristic absorbance feature, confirm the successful preparation of $Au_{36}(PA)_{24}$ [21]. However, the formation process of $Au_{36}(PA)_{24}$ has not been uncovered, which is one of the major goal of our study. To achieve such goal, one viable choice is that slowing down the reaction process and identifying the key intermediate, which will be discussed next.

To track the intermediate, manipulating the reaction kinetics is critical. Note that, compared with $NaBH_4$, $NaBH_3CN$ possesses lower reducing capability with slower reaction rate, plus ice bath to maintain zero temperature, the reaction environment is very mild. During the Au_{36} synthesis, we observed an obvious color change from colorless to red and finally to green. By reducing the amount of $NaBH_3CN$ (1/3 eq. per Au) and sampling to purify by PTLC, the bright red solid was isolated. The composition of the intermediate was determined by MALDI-MS measurement. As presented in Figure 1(b), the spectrum shows a main peak located at *m*/*z*=4,962.01 Da, corresponding to $Au_{18}(PA)_{14}$ (theoretical MW: 4,961.19 Da, deviation: 0.82 Da). Note that, in the recent study by Tsukuda *et al*. [17], the major peak for $Au_{22}(PA)_{18}$ is also $Au_{18}(PA)_{14}$, as $Au_4(PA)_4$ can be easily lost in MADLI-MS test in reflection negative mode (Figure S2(a)). Such phenomenon has been previously documented in thiolated Au nanoclusters as well [39,40], for instance, in the MS spectra of $Au_{25}(SR)_{18}$, $Au_{21}(SR)_{14}$ is always one major peak with high intensity in several reports [41–43]. In fact, in our case, the molecular ion peak in reflection positive mode (Figure S2(b)) is weak but still identifiable. The molecular ion (*m*/*z*=6,153.71 Da) agrees well with the calculated value (MW: 6,153.57 Da), further verifies the intermediate for forming Au_{36} is Au_{22}. According to the peak assignment analysis in Table S1, main fragments are ranging from $[Au_{22}(PA)_{17}]^+$ to $Au_{17}(PA)_{13}^+$. The absorbance profile of $Au_{22}(PA)_{18}$ is depicted in Figure 1(d), where a characteristic peak at 475 nm and a broad band at 531 nm are readily observable. The inset of Figure 1(d) shows the photograph of the Au_{22} solution and the optical absorbance profile with photoenergy as *x* axis. The absorbance feature and the calculated bandgap of 2.17 eV agree well with the recent report [17].

We also found some intriguing phenomenon in the synthesis of $Au_{22}(PA)_{18}$. During the injection course of

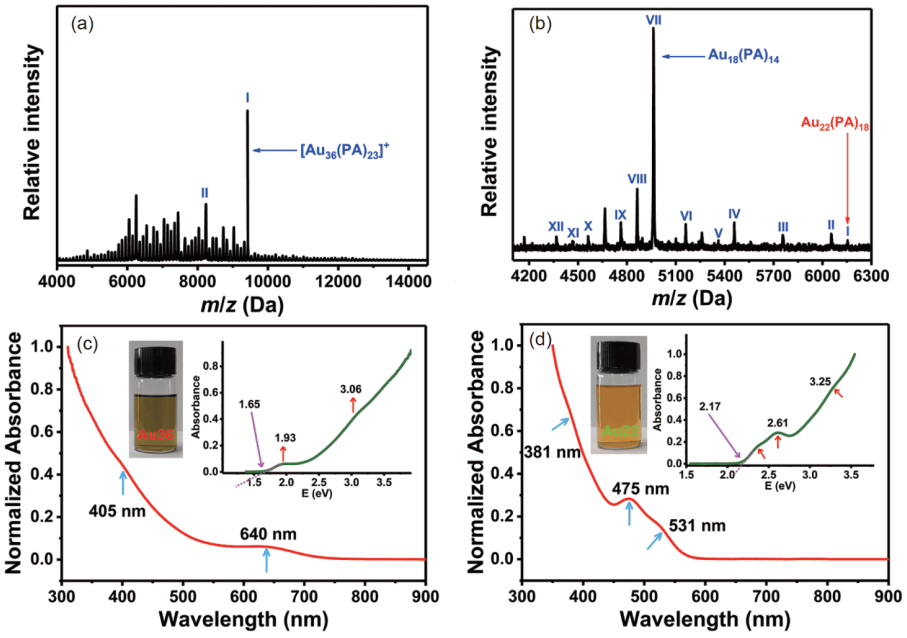

Figure 1 MALDI-MS (a, b) and absorption spectra (c, d) of $Au_{36}(PA)_{24}$ and $Au_{22}(PA)_{18}$, respectively. Insets are the spectra plotted in energy axis and the photos of $Au_{36}(PA)_{24}$ and $Au_{22}(PA)_{18}$ in CH_2Cl_2, respectively (color online).

ligand and $NaBH_3CN$, the reaction mixture changed gradually from colorless to light yellow, and then turned into yellow suspension. Finally, the yellow suspension changed into orange-red solution (Au_{22}), and the whole process can be completed in less than 15 min. It suggests that Au_{22} can be formed very fast, and the calculated yield is ~70.8%. Note that, in the recent report, the yield of $Au_{22}(PA)_{14}$ was ~8% in more than 1 h reaction time [17], while in another study of $Au_{22}(^tBuC{\equiv}C)_{18}$, the yield was ~29%, regardless the slight difference of the ligand [18]. The much less reaction time and markedly higher yield highlight the advantages of our synchronous nucleation and passivation strategy.

3.2 The stochiometric synthesis to elucidate the reaction kinetics

To further elucidate the Au nanoclusters formation process and differentiate the product species, stoichiometric synthesis with precise control of the $NaBH_3CN$ amount was conducted (Scheme 1). Different quantities (3 eq., 1 eq., 1/2 eq., 1/3 eq. per Au) of $NaBH_3CN$ were employed, and the time-resolved absorbance spectra are presented in Figure 2. With 3 eq. $NaBH_3CN$, featureless exponential decay absorbance profile with almost no change during the whole reaction period can be observed (Figure 2(a)), suggesting polydisperse Au nanoclusters were produced. To identify the compositions of these species, the MALDI MS test in positive mode was conducted and shown in Figure S3. Compared with the matrix (DCTB), there are mainly three major species at m/z<5,000 in the mixture. As shown in Figure S3(a), the peaks of a and b are the fragments of the parental nanoclusters, and the peak of c can be assigned to $Au_6(PA)_5^+$, as will be discussed next. MALDI-MS spectra reveal that as-prepared product is a mixture of $Au_n(C{\equiv}CPh)_m$, where some of them can be potentially assigned as (n, m)=(38, 24), (42, 20), (42, 22), (68, 32), and (76, 44) (Figure S3(b)). However, when the amount of $NaBH_3CN$ was cut down to 1 eq. (Figure 2(b)), 1/2 eq. (Figure 2(c)), and 1/3 eq. (Figure 2(d)), different absorbance features can be obtained, and all the absorbance changed with time and finally stabilized in 24 h. Specifically, for the 1 eq. trial, there is a strong absorbance peak at 595 nm in 10 min. Besides that, 640 nm characteristic absorbance peak from Au_{36} can also be identified. Interestingly, the 595 nm absorbance peak gradually decreases while the Au_{36} feature increases in 24 h. The species bearing 595 nm absorbance peak was successfully isolated. A series of characterization was then conducted to reveal its identity and the composition was first determined by MALDI-MS detection in reflection positive mode. As presented in Figure S4, a main peak is located at m/z=1,687.22 Da, corresponding to $Au_6(PA)_5^+$ (theoretical MW: 1,687.44 Da, deviation: 0.22 Da). $Au_6(PA)_5^+$ is likely derived from the removal of an alkynyl group (–C≡CPh) from the parental $Au_6(PA)_6$ (Au_6 in short), and such one PA ligand removal phenomenon has been previously observed in the MALDI-MS spectra of $Au_{36}(PA)_{24}$ and $Au_{44}(PA)_{28}$ nanoclusters as well [21]. It indicates the species bearing the 595 nm characteristic absorbance peak is $Au_6(PA)_6$. To further verify its

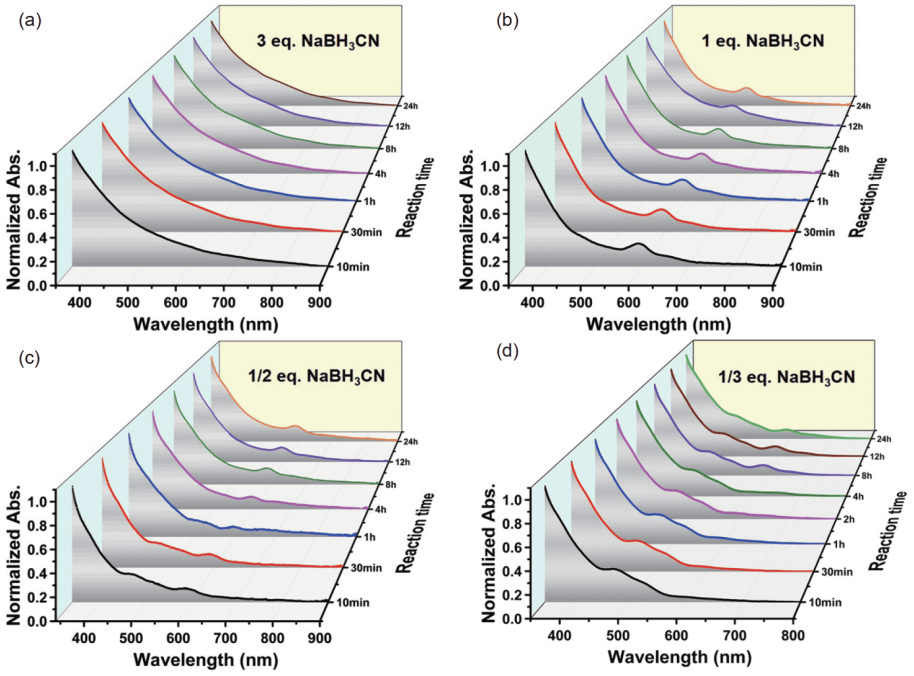

Figure 2 The absorbance change upon the addition of different amounts of $NaBH_3CN$ at different time (10 min, 30 min, 1 h, 4 h, 8 h, 12 h, 24 h). (a) 3 eq. per Au; (b) 1 eq. per Au; (c) 1/2 eq. per Au; (d) 1/3 eq. per Au. An aliquot of the reaction mixture in methylene chloride phase was diluted to the proper absorbance range for each measurement. The spectra are normalized at 350 nm (color online).

identity, the X-ray photoelectron spectroscopic survey scan spectra of the Au_6 complex is recorded and shown in Figure S5(a), where only the key elements of Au and C can be observed. It rules out the possibility of the presence of Cl in the $Au_6(PA)_6$ [44]. Moreover, as shown in Figure S5(b), the Au atoms in $Au_6(PA)_6$ is +1 valence from the core-level XPS spectra of the Au 4f electrons [45,46], suggesting that $Au_6(PA)_6$ is an Au(I) complex. TGA was further conducted to verify its composition. As shown in Figure S6, a total weight loss of 33.80% was observed. From the Au/PA mass ratio, the formula of the Au_6 complex can be further confirmed as $Au_6(PA)_6$ (calculated Au/PA mass ratio is 66.11:33.89). From the above results, $Au_6(PA)_6$ has been proved to be an homoleptic complex, and it may have a ring structure or even be involved in catenane structures [47,48].

In addition, for the 1/2 eq. trial, both the Au_6 and Au_{36} features appeared in 10 min, but the Au_{36} content increased while the Au_6 ratio diminished in 24 h. Interestingly, for the 1/3 eq. trial, the Au_{22} feature dominated the absorbance profile with a trace amount of Au_{36} in 10 min. The reaction can be terminated, and $Au_{22}(PA)_{18}$ can be isolated and the yield was calculated as ~70.8%. With the time increasing, the final product for this trial exhibited both Au_6 and Au_{36} features. One can conclude that, the stoichiometric ratio of $NaBH_3CN$-to-Au significantly affects the composition of the initial and final products.

3.3 Proposed structural evolution from Au_{22} to Au_{36}

Since the absorbance profile and feature of $Au_{22}(PA)_{18}$ are almost identical with the other alkynyl-protected $Au_{22}L_{18}$ (L–H=3-ethynylthiophene [17], and 3,3-dimethyl-1-butyne [18]) nanoclusters with structure disclosed by SCXRD, the architecture of the Au core in $Au_{22}(PA)_{18}$ is presumably the same with these two Au_{22} nanoclusters. Plus the defined $Au_{36}(PA)_{24}$ structure, a tentative Au core structure evolution model has been postulated. As shown in Figure 3(a), in the Au core of $Au_{22}(PA)_{18}$, Au_7 kernel and $Au_6(PA)_6$ ring form a distorted Au_{13} cuboctahedron. Such distorted octahedron has been reported in $Au_{23}(SR)_{16}$ [49] and $[Au_{24}(PA)_{14}(PPh_3)_4]^{2+}$ [26]. The extra free PA ligand can react with the PA on the $Au_6(PA)_6$ ring in the distorted Au_{13} core, plus the strong aurophilic interaction of the Au atoms [50], result in Au–Au bond formation at the external of the Au_{13} core (see transition state in Figure 3(a)), and can eventually lead to the formation of a Au_{13} cuboctahedron. Subsequently, two Au_{13} cuboctahedra are fused together forming an Au_{20} subunit along with a loss of 6 Au atoms (Figure 3(b)). Finally, two Au_{20} subunits can interpenetrate with each other, leading to the formation of an Au_{28} core with 12 Au atoms stripped off.

It is worth pointing out that, from Au_{22} to Au_{36}, the generation of $Au_6(PA)_6$ is inevitable, but it can also be employed as an effective indicator for the whole Au core evolution process. Firstly, two Au_{13} cuboctahedra interpenetrate to form a Au_{20} subunit along with the release of six Au atoms, which can immediately react with six PA molecules in the solution, forming one $Au_6(PA)_6$ molecule. Following that, two Au_{20} subunits can interpenetrate with each other to generate a Au_{28} core, accompanying with the stripping of 12 Au atoms, which yields two $Au_6(PA)_6$ molecules as well.

Since the intermediate $Au_{22}(PA)_{18}$ can eventually yield $Au_{36}(PA)_{24}$, $Au_6(PA)_6$, and a small amount of $Au_{22}(PA)_{18}$ left, based on the above structure evolution model, in the 1/3 eq. trial, the quantative relationship can be proposed (Eq. (1)):

$$a[Au_{22}(PA)_{18}] = b[Au_{36}(PA)_{24}] + c[Au_6(PA)_6] + d[Au_{22}(PA)_{18}] \quad (1)$$

where a, b, c and d represent the reaction coefficients of

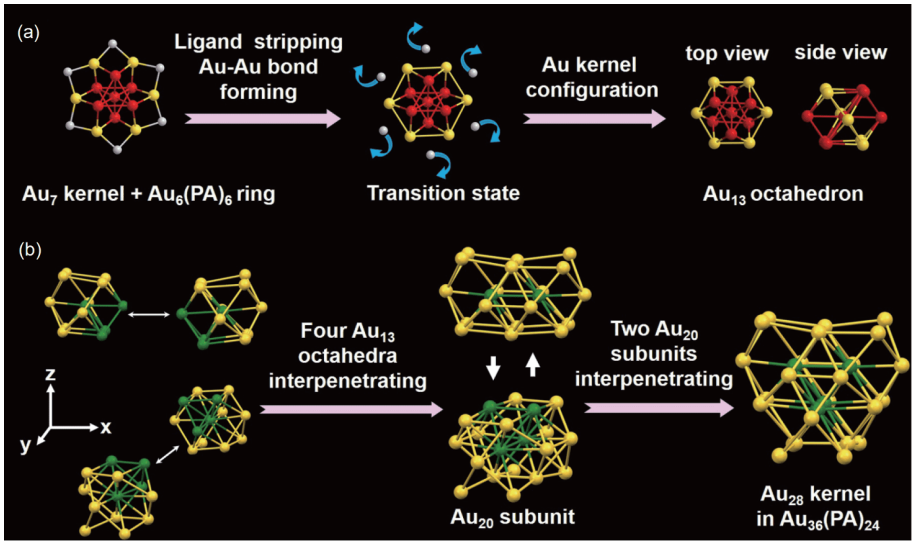

Figure 3 Structure evolution from Au_{22} to Au_{36}. (a) The transformational diagram from Au_7 kernel and $Au_6(PA)_6$ ring to Au_{13} cuboctahedron. (b) Four Au_{13} cuboctahedra interpenetrating to form a Au_{28} kernel of Au_{36}. Color labels: yellow, Au; green, the central Au atom in Au_{13} (color online).

Au_{22}, Au_{36}, Au_6, and residual Au_{22} respectively. As each Au_{22} molecule contains one Au_{13} core, while four Au_{13} cores can form two Au_{20} subunits which interpenetrate together as one Au_{28} core, that means, the stochiometric ratio of the gold core in Au_{22}-to-Au_{36} is 4:1 (a/b=4:1).

In addition, the number of Au atoms and PA ligands in the Au_{22} and Au_{36} nanoclusters could be illustrated in Eqs. (2, 3):

$$Au_{22}(PA)_{18} = Au_7 + [Au_6(PA)_6] + 3[Au_3(PA)_4] \quad (2)$$

$$Au_{36}(PA)_{24} = Au_{28} + 4[Au_2(PA)_3] + 12PA \quad (3)$$

From Eqs. (2, 3), futher derivation can be achieved as follows:

$$\begin{aligned} 4Au_{22}(PA)_{18} &= 4\{Au_7 + [Au_6(PA)_6] + 3[Au_3(PA)_4]\} \\ &= 4\{Au_{13} + 6PA + 3[Au_3(PA)_4]\} \\ &= Au_{28} + 24Au + 24PA + 12[Au_3(PA)_4] \\ &= \{Au_{28} + 4[Au_2(PA)_3] + 12PA\} \\ &\quad + 5[Au_6(PA)_6] \\ &\quad + \{Au_{13} + 6PA + 3[Au_3(PA)_4]\} \\ &= Au_{36}(PA)_{24} + 5[Au_6(PA)_6] + Au_{22}(PA)_{18} \end{aligned} \quad (4)$$

To that end, $a/b/c/d$=4:1:5:1. And the simplified stoichiometric ratio of Au_{22}-to-Au_{36} was 3:1.

3.4 The experimental intermediate/product ratio confirmation

To verify the above stoichiometric ratio of Au_{22}-to-Au_6-to-Au_{36}, the absorbance change in the 1/3 eq. trial was further quantified. Figure 4(a) shows the photos of the three purified clusters of Au_{22} (c=4.81×10^{-6} M), Au_{36} (c=2.27×10^{-6} M), and Au_6 (c=8.10×10^{-6} M) dissolved in 10 mL CH_2Cl_2. Given the standard absorbance curve of the three species, according to Lambert-Beer's law, the molecular absorptivity (ε) of Au_{22} (ε=0.2×10^5 M^{-1} cm^{-1}) (Figure 4(b)), Au_{36} (1.08×10^5 M^{-1} cm^{-1}) (Figure 4(c)), and Au_6 (0.21×10^5 M^{-1} cm^{-1}) (Figure 4(d)) can be determined, as summarized in Table S3. Using the 475, 640 and 595 nm absorbance peak value as the fingerprint metric for Au_{22}, Au_{36}, and Au_6, respectively, for the 1 eq. trial, the absorbance changes from 10 min to 24 h can be quantified and employed to verify the Au_{22}-to-Au_6-to-Au_{36} ratio. During the whole process, the absorbance (concentration) changes of three species are summarized in Table S4. As above, the concentration decrease of Au_{22} was 1.18×10^{-6} M, accompanying with the concentration augment of Au_6 (1.92×10^{-6} M) and Au_{36} (0.40×10^{-6} M), respectively. Therefore, the calculated stoichiometric ratio of Au_{22}-to-Au_6-to-Au_{36} is 2.9:4.8:1, which agrees well with the theoretical value proposed based on the structure evolution model. It attests the validity of our proposed structure evolution model. Furthermore, the ultimate yields of Au_{22} and Au_{36} clusters in reaction mixture can be accurately determined according to their characteristic absorption curve (Figures S7 and S8), which are up to 70.8% and 17.1%, respectively.

4 Conclusions

In conclusion, a novel synchronous nucleation and passiva-

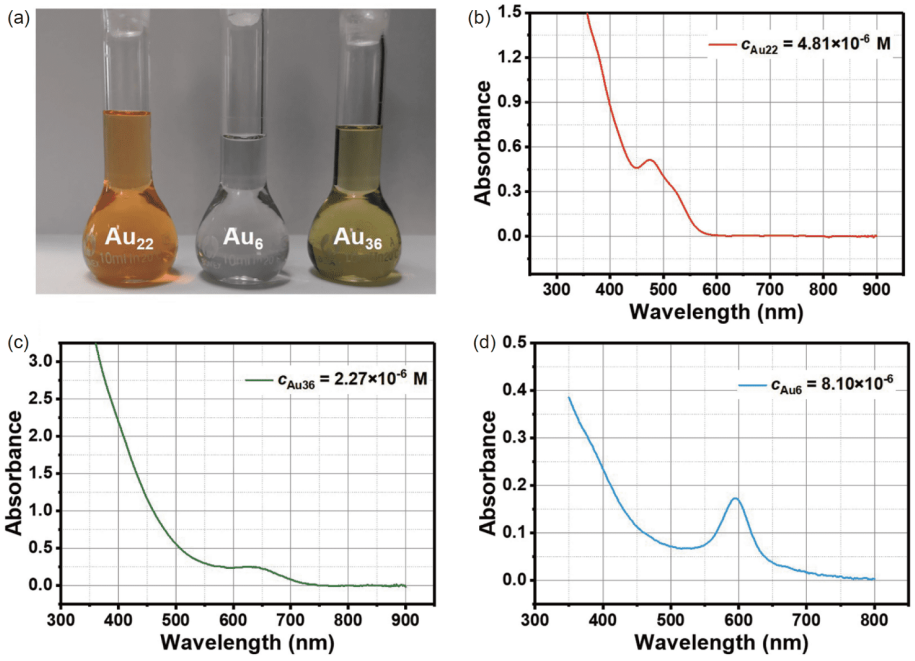

Figure 4 (a) The photos of the purified products in 10 mL CH_2Cl_2; the molar absorptivity (ε) determined by the standard absorption curve of the isolated $Au_{22}(PA)_{18}$ (b), $Au_{36}(PA)_{24}$ (c), and $Au_6(PA)_6$ (d) (color online).

tion strategy is devloped to fabricate $Au_{36}(PA)_{24}$ and $Au_{22}(PA)_{18}$ molecules with high yield (>17% for Au_{36}, >70% for Au_{22}) by employing $NaBH_3CN$ as reducing agent at low temperature. Au_{22} has been identified as the key intermediate for forming Au_{36}, while $Au_6(PA)_6$ complex is generated during the process. The structure evolution model from Au_{22} to Au_{36} has been proposed, and based on that, the stoichiometric ratio of $Au_{22}/Au_{36}/Au_6$ can be calculated, which is further verified by the experimental results. This study not only provides a novel strategy for controlled synthesis of homoleptic alkynyl-protected Au nanoclusters with high yields, but also sheds light on understanding the structural evolution process of alkynyl-protected Au nanoclusters at atomic level. Further efforts to extend this method to acquire other coinage metal clusters with alkynyl protection are underway in our lab.

Acknowledgements This work was supported by Guangdong Natural Science Funds for Distinguished Young Scholars (2015A030306006), Guangzhou Science and Technology Plan Projects (201804010323), the fundamental funds for central universities (SCUT, 2018ZD022), and the National Natural Science Foundation of China (21971070).

Conflict of interest The authors declare no conflict of interest.

Supporting information The supporting information is available online at http://chem.scichina.com and http://link.springer.com/journal/11426. The supporting materials are published as submitted, without typesetting or editing. The responsibility for scientific accuracy and content remains entirely with the authors.

1 Wang S, Yu H, Zhu M. *Sci China Chem*, 2015, 59: 206–208
2 Yao Q, Chen T, Yuan X, Xie J. *Acc Chem Res*, 2018, 51: 1338–1348
3 Jin R, Zeng C, Zhou M, Chen Y. *Chem Rev*, 2016, 116: 10346–10413
4 Higaki T, Li Q, Zhou M, Zhao S, Li Y, Li S, Jin R. *Acc Chem Res*, 2018, 51: 2764–2773
5 Kang X, Zhu M. *Chem Soc Rev*, 2019, 48: 2422–2457
6 Yan J, Teo BK, Zheng N. *Acc Chem Res*, 2018, 51: 3084–3093
7 Gan Z, Xia N, Wu Z. *Acc Chem Res*, 2018, 51: 2774–2783
8 Wang Z, Qu QP, Su HF, Huang P, Gupta RK, Liu QY, Tung CH, Sun D, Zheng LS. *Sci China Chem*, 2019, 63: 16–20
9 Yuan X, Luo Z, Yu Y, Yao Q, Xie J. *Chem Asian J*, 2013, 8: 858–871
10 Wu XH, Wei Z, Yan BJ, Huang RW, Liu YY, Li K, Zang SQ, Mak TCW. *CCS Chem*, 2019, 1: 553–560
11 Yan J, Zhang J, Chen X, Malola S, Zhou B, Selenius E, Zhang X, Yuan P, Deng G, Liu K, Su H, Teo BK, Häkkinen H, Zheng L, Zheng N. *Natl Sci Rev*, 2018, 5: 694–702
12 Du Y, Sheng H, Astruc D, Zhu M. *Chem Rev*, 2020, 120: 526–622
13 Chen S, Ma H, Padelford JW, Qinchen W, Yu W, Wang S, Zhu M, Wang G. *J Am Chem Soc*, 2019, 141: 9603–9609
14 Jia TT, Yang G, Mo SJ, Wang ZY, Li BJ, Ma W, Guo YX, Chen X, Zhao X, Liu JQ, Zang SQ. *ACS Nano*, 2019, 13: 8320–8328
15 Zheng K, Setyawati MI, Leong DT, Xie J. *ACS Nano*, 2017, 11: 6904–6910
16 Yan L, Yu Y, Xia Z. *Sci China Chem*, 2018, 61: 619–626
17 Ito S, Takano S, Tsukuda T. *J Phys Chem Lett*, 2019, 10: 6892–6896
18 Han XS, Luan X, Su HF, Li JJ, Yuan SF, Lei Z, Pei Y, Wang QM. *Angew Chem Int Ed*, 2020, 59: 2309–2312
19 Guan ZJ, Hu F, Li JJ, Wen ZR, Lin YM, Wang QM. *J Am Chem Soc*, 2020, 142: 2995–3001
20 Li JJ, Guan ZJ, Lei Z, Hu F, Wang QM. *Angew Chem*, 2019, 58: 1083–1087
21 Wan XK, Guan ZJ, Wang QM. *Angew Chem Int Ed*, 2017, 56: 11494–11497
22 Guan ZJ, Hu F, Li JJ, Liu ZR, Wang QM. *Nanoscale*, 2020, 12: 13346–13350
23 Lei Z, Li JJ, Wan XK, Zhang WH, Wang QM. *Angew Chem Int Ed*, 2018, 57: 8639–8643
24 Wan XK, Tang Q, Yuan SF, Jiang D, Wang QM. *J Am Chem Soc*, 2015, 137: 652–655
25 Wan XK, Yuan SF, Tang Q, Jiang D, Wang QM. *Angew Chem Int Ed*, 2015, 54: 5977–5980
26 Wan XK, Xu WW, Yuan SF, Gao Y, Zeng XC, Wang QM. *Angew Chem Int Ed*, 2015, 54: 9683–9686
27 Wan XK, Wang JQ, Nan ZA, Wang QM. *Sci Adv*, 2017, 3: e1701823
28 Wang T, Zhang WH, Yuan SF, Guan ZJ, Wang QM. *Chem Commun*, 2018, 54: 10367–10370
29 Tang Q, Hu G, Fung V, Jiang DE. *Acc Chem Res*, 2018, 51: 2793–2802
30 Lei Z, Wan XK, Yuan SF, Guan ZJ, Wang QM. *Acc Chem Res*, 2018, 51: 2465–2474
31 Lei Z, Wang QM. *Coord Chem Rev*, 2019, 378: 382–394
32 Maity P, Wakabayashi T, Ichikuni N, Tsunoyama H, Xie S, Yamauchi M, Tsukuda T. *Chem Commun*, 2012, 48: 6085–6087
33 Wang Y, Su H, Xu C, Li G, Gell L, Lin S, Tang Z, Häkkinen H, Zheng N. *J Am Chem Soc*, 2015, 137: 4324–4327
34 Gupta AK, Orthaber A. *Chem Eur J*, 2018, 24: 7536–7559
35 Ma X, Tang Z, Qin L, Peng J, Li L, Chen S. *Nanoscale*, 2020, 12: 2980–2986
36 Hooper TN, Butts CP, Green M, Haddow MF, McGrady JE, Russell CA. *Chem Eur J*, 2009, 15: 12196–12200
37 CrysAlisPro. User Manual for Version 1.171.35.19, 2011
38 Dolomanov OV, Bourhis LJ, Gildea RJ, Howard JAK, Puschmann H. *J Appl Crystlogr*, 2009, 42: 339–341
39 Tsunoyama R, Tsunoyama H, Pannopard P, Limtrakul J, Tsukuda T. *J Phys Chem C*, 2010, 114: 16004–16009
40 Tang Z, Xu B, Wu B, Robinson DA, Bokossa N, Wang G. *Langmuir*, 2011, 27: 2989–2996
41 Dass A, Stevenson A, Dubay GR, Tracy JB, Murray RW. *J Am Chem Soc*, 2008, 130: 5940–5946
42 Zhu M, Eckenhoff WT, Pintauer T, Jin R. *J Phys Chem C*, 2008, 112: 14221–14224
43 Liu C, Lin S, Pei Y, Zeng XC. *J Am Chem Soc*, 2013, 135: 18067–18079
44 Chen Y, Zeng C, Kauffman DR, Jin R. *Nano Lett*, 2015, 15: 3603–3609
45 Tang Z, Robinson DA, Bokossa N, Xu B, Wang S, Wang G. *J Am Chem Soc*, 2011, 133: 16037–16044
46 Negishi Y, Nobusada K, Tsukuda T. *J Am Chem Soc*, 2005, 127: 5261–5270
47 Bertorelle F, Russier-Antoine I, Calin N, Comby-Zerbino C, Bensalah-Ledoux A, Guy S, Dugourd P, Brevet PF, Sanader Ž, Krstić M, Bonačić-Koutecký V, Antoine R. *J Phys Chem Lett*, 2017, 8: 1979–1985
48 Comby-Zerbino C, Perić M, Bertorelle F, Chirot F, Dugourd P, Bonačić-Koutecký V, Antoine R. *Nanomaterials*, 2019, 9: 457
49 Das A, Li T, Nobusada K, Zeng C, Rosi NL, Jin R. *J Am Chem Soc*, 2013, 135: 18264–18267
50 Wu Z, Du Y, Liu J, Yao Q, Chen T, Cao Y, Zhang H, Xie J. *Angew Chem Int Ed*, 2019, 58: 8139–8144